Analysis of the valence-band photoemission spectrum of Sr$_2$CuO$_2$Cl$_2$ along the high-symmetry directions

R. Hayn and H. Rosner

Institute for Theoretical Physics, TU Dresden, D-01062 Dresden, Germany

V. Yu. Yushankhai

Joint Institute for Nuclear Research, 141980 Dubna, Moscow Region, Russia

S. Haffner, C. Dürr, M. Knupfer, G. Krabbes, M. S. Golden, J. Fink, and H. Eschrig

Institute for Solid State and Materials Research (IFW) Dresden, P. O. Box 270016, D-01171 Dresden, Germany

D. J. Singh

Complex Systems Theory Branch, Naval Research Laboratory, Washington, DC 20375-8795

N. T. Hien and A. A. Menovsky

Van der Waals–Zeeman Laboratory, University of Amsterdam, Valckenierstraat 65, 1018 XE, Amsterdam, The Netherlands

Ch. Jung and G. Reichardt

BESSY GmbH, Lentzeallee 100, D-14195 Berlin, Germany

Band structure calculations have been used to identify the different bands contributing to the polarization-dependent photoemission spectra of the undoped model cuprate Sr$_2$CuO$_2$Cl$_2$ at the high-symmetry points of the CuO$_2$ plane Γ, $(\pi/a,0)$ and $(\pi/a,\pi/a)$ and along the high-symmetry directions $\Gamma-(\pi/a,\pi/a)$ and $\Gamma-(\pi/a,0)$. Results from calculations within the local density approximation (LDA) have been compared with calculations taking into account the strong electron correlations by LDA+U, with the result that the experimental order of energy levels at the high-symmetry points is better described by the LDA+U calculation than by the simple LDA. All the main peaks in the photoemission spectra at the high symmetry points could be assigned to different Cu $3d$ and O $2p$ orbitals which we have classified according to their point symmetries. The dispersions along the high-symmetry directions were compared with an 11-band tight-binding model which was fitted both to the LDA+U band structure calculation and the angle-resolved photoemission data. The mean field treatment successfully describes the oxygen derived bands but shows discrepancies for the copper ones. [S0163-1829(99)01925-6]

I. INTRODUCTION

One strategy to answer the many questions concerning the electronic structure of cuprate superconductors is the study of model substances. One of these compounds is Sr$_2$CuO$_2$Cl$_2$. It is a two dimensional (2D) antiferromagnetic (AFM) insulator with a Néel temperature[1] of 256 K whose magnetic structure is well described by the 2D spin-1/2 Heisenberg model. It was the first undoped cuprate which allowed the angle resolved photoemission (ARPES) measurement of its lowest excitations.[2–4] These excitations are well described by one hole in a 2D quantum antiferromagnet.[5–7] Deviations from the one-hole dispersion of the pure t-J model can be reduced by taking into account hopping terms to second and third neighbors.[8,9] In the same substance the low binding energy edge of the main valence band has been interpreted in terms of nonbonding oxygen orbitals which are completely decoupled from the copper system.[10] (These features were known before as ''1 eV peak.''[11]) These non-bonding states are especially pronounced at (π,π) where they have minimal binding energy. But the detailed structure of the complete valence band has

never been analyzed up to now and that is the aim of the present work. Furthermore, we will show that one can obtain additional information on the low binding-energy features by analyzing their dependence on the polarization of the photon.

Polarization dependent photoemission measurements are an effective tool to analyze the electronic structure of the valence band in detail. By measuring along high-symmetry directions all bands can be classified according to their symmetry properties. This allows a very precise comparison between experiment and different theoretical predictions. It is well established that in all the cuprates electron correlations have a strong influence on the electronic bands near the Fermi level which is especially pronounced in undoped substances.[6] But the influence of correlations on those parts of the valence band with larger binding energies is less clear. We will show that the combination of polarization dependent ARPES measurements with theoretical investigations taking into account the electron correlation to a differing extent (LDA, LDA+U) provides a unique possibility to answer this question.

The model cuprate Sr$_2$CuO$_2$Cl$_2$ is very well suited for such an investigation. It has a tetragonal structure with ideal

planar CuO_2 layers[12] and cleaves readily parallel to the CuO_2 planes. Furthermore, the presence of Cl instead of apex oxygen allows a restriction of the states which contribute to the ARPES spectra to those of the pure CuO_2 plane alone. This can be achieved by choosing a photon energy close to the Cooper minimum for Cl $3p$ photoemission, i.e., Cl $3p$ states will then have a small photon cross section. In this manner we intend to study an ideal situation whose main characteristics should be generic to all the cuprates.

Recently, a similar study was presented for the Cu_3O_4 plane of $Ba_2Cu_3O_4Cl_2$.[13] It turns out that $Sr_2CuO_2Cl_2$ is considerably less complex than $Ba_2Cu_3O_4Cl_2$. Therefore, we are now able to identify *all* the peaks at the high symmetry points in contrast to $Ba_2Cu_3O_4Cl_2$ where only the upper parts of the valence band were analyzed. This allows implications about the influence of electron correlations on the valence band (VB) structure of $Sr_2CuO_2Cl_2$ to be made. It is known that simple LDA fails to predict the insulating ground state of undoped cuprates.[14] There are several improvements of LDA such as the self-interaction correction (SIC) method[15] or LDA+U[16], which has already been applied to the case of lanthanum cuprate[17] (La_2CuO_4). Here, we apply LDA+U plus a symmetry analysis at special k points to interprete the polarization dependent photoemission data for $Sr_2CuO_2Cl_2$, where the actual value of U is chosen to describe the experimental situation.

The paper is organized as follows. After describing the experimental method and the details of the LDA band structure calculation we analyze the symmetry properties of the wave function along high-symmetry directions. The symmetry properties of the relevant bands are most clearly seen in a tight-binding model presented in Sec. IV. Discussing the correlation effects in a mean-field manner leads us to an LDA+U calculation whose results are presented in Sec. V. In Sec. VI we compare the experimental spectra with the theoretical predictions. The spectra at Γ, $(\pi,0)$ and (π,π) (the lattice constant has been set to unity in all the notations) can be understood from the LDA+U but not from the LDA calculation. The experimental dispersion relations are discussed in terms of a tight-binding (TB) model.

II. EXPERIMENTAL

The $Sr_2CuO_2Cl_2$ single crystals were grown from the melt, their typical dimensions being $3\times3\times0.5$ mm. The crystals were mounted on the sample holders using conducting, or in some cases, insulating epoxy. If insulating epoxy was used, electrical contact between sample holder and sample was achieved by means of a graphite layer at the sides of the crystal. The orientation of the single crystals was determined *ex situ* by x-ray diffraction. The surface normal of the crystals is perpendicular to the CuO_2 planes. Prior to the ARPES measurements, a clean crystal surface was prepared in ultra high vacuum (UHV) by stripping off an adhesive tape which was attached on the sample surface.

The ARPES measurements were performed using linearly polarized 35 eV photons from the crossed undulator beamline U2 of the BESSY I facility and BESSY's HIRES photoelectron spectrometer.[18] The angular resolution was set to $\pm1°$ which gives a momentum resolution of ±0.05 Å^{-1} for states of 1 eV binding energy, this corresponds to 12% of the
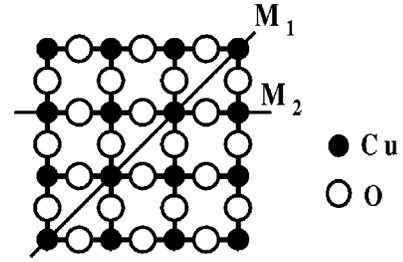
FIG. 1. The mirror planes of the CuO_2 plane. Filled (open) circles correspond to copper (oxygen) atoms.

distance between Γ and $(\pi,0)$. A total energy resolution (resulting from both the monochromator and electron analyzer resolutions) of 150 meV was applied. The electron analyzer is fixed in the horizontal plane at an angle of 60° with respect to the incoming photon beam, i.e., the emission plane which is defined to be the plane spanned by the sample surface normal and the k vectors of the measured photoelectrons, is always a horizontal plane. The photoelectron momentum vector could then be changed by variation of the angle between the axis of the input lens of the electron analyzer and the sample surface normal by rotation of the manipulator on which the sample holder was mounted. The ARPES spectra have been recorded in the electron distribution curve (EDC) mode from both Γ to (π,π) and Γ to $(\pi,0)$. In the latter case, the sample was oriented in such a way that the Cu-O bonds of the CuO_2 plane were aligned parallel to the fixed, horizontal emission plane, while in the former case, the Cu-O bonds were aligned at an angle of 45° with respect to the emission plane. The spectra are normalized with respect to the incoming photon flux which was simultaneously measured using the drain current of a gold mesh. The absolute binding energy scale was determined according to $E_B = h\nu - E_{kin} - \phi_{analyzer}$ using the photon energy, the measured kinetic energy of the photoelectrons and the known analyzer work function. There were no indications of charging-induced energy shifts. All spectra were recorded at 300 K within 8 hours of a cleave, during which time the samples showed no indications of surface degradation.

The electronic structure of the VB is derived from O $2p$, Cu $3d$, and Cl $3p$ orbitals, but for 35 eV photon energy, the photoionization cross section of the Cl $3p$ orbitals is much smaller than that of the O $2p$ and Cu $3d$ orbitals,[19] which therefore dominate the ARPES VB spectra. The measurements had been performed at room temperature which is slightly above the Neél temperature of $Sr_2CuO_2Cl_2$ (256 K). Although we are aware that AFM fluctuations are important, we nevertheless analyzed the spectra in terms of the first Brillouin zone (BZ) of the paramagnetic CuO_2 plane of $Sr_2CuO_2Cl_2$. We will see that this is especially justified for the bands with dominant oxygen character, whereas one observes some deviations for those bands which couple strongly with the copper spins. The geometrical structure of a CuO_2 plane has two mirror planes (denoted M_1 and M_2 in Fig. 1).[20] All the bands with a wave vector between Γ and (π,π), parallel to the mirror plane M_1, can be classified to be either symmetric or antisymmetric with respect to M_1, and analogously also for wave vectors along $\Gamma-(\pi,0)$ with respect to reflections at M_2. Experimental information about

the parity of the valence band states with respect to a mirror plane can be obtained by recording the ARPES spectra with either perpendicular or parallel polarization of the electric field vector of the incoming radiation with respect to an emission plane which is parallel to a mirror plane of the system. It can then be shown[21] that for parallel polarization only initial valence band states which are even with respect to the emission/mirror plane contribute to an ARPES spectrum while for perpendicular polarization, only states which are odd with respect to the emission/mirror plane are seen in a spectrum. In this work, the polarization of the electric field vector was chosen by using either the vertical or horizontal undulator, which corresponds to perpendicular and parallel polarization with respect to the emission plane. The emission plane is parallel to mirror plane M_1, if the ARPES spectra are recorded along the (π,π) direction, while it is parallel to the mirror plane M_2 for spectra along the $(\pi,0)$ direction. For perpendicular polarization, the electric field vector is always parallel to the CuO_2 planes, i.e., only in-plane orbitals as O $2p_{x,y}$ or Cu $3d_{x^2-y^2}$ contribute to the spectra. For parallel polarization, the electric field vector is completely in-plane only at normal-incidence, at any other incidence angle of the photon beam, the electric field vector has an out-of-plane component and there are also contributions from out-of-plane orbitals such as O $2p_z$ to the ARPES spectra.

III. BAND STRUCTURE CALCULATIONS

$Sr_2CuO_2Cl_2$ has a body centered tetragonal crystal structure with the lattice constants $a=3.973$ Å and $c=15.618$ Å.[12] Band structure calculations have been performed treating the exchange and correlation potential within the local density approximation (LDA). The Bloch wave functions were constructed from atomiclike wave functions according to the linear combination of atomic orbitals (LCAO) method. The calculation was scalar relativistic and due to the open crystal structure two empty spheres per elementary cell were introduced in between two oxygen atoms of neighboring CuO_2 planes. A minimal basis was chosen consisting of $Sr(5s,5p,4d)$, $Cu(4s,4p,3d)$, $O(2s,2p)$, $Cl(3s,3p)$ orbitals and the $1s$ and $2p$ orbitals for the empty spheres. To optimize the local basis a contraction potential $(r/r_0)^4$ was introduced.[22] The Coulomb potential is constructed as a sum of overlapping contributions of spherical symmetry and for the exchange and correlation potential the atomic sphere approximation (ASA) is used.

In the resulting band structure (Fig. 2) one observes an antibonding band built up of Cu $3d_{x^2-y^2}$ and O $2p_{x,y}$ orbitals crossing the Fermi level. This contradicts the experimentally observed nonmetallic behavior which already indicates that one has to treat the electron correlations in a more explicit way. One could conjecture that the only effect of correlations is to split the half-filled antibonding band leaving the structure of the other valence bands roughly unchanged. That is not the case, however, as will become clear from our following analysis. One can also observe in Fig. 2 that there is nearly no dispersion of the relevant band in the z direction and all discussions in the present paper will be restricted to the CuO_2 plane only.

To check the minimal basis LCAO method, a full potential linearized augmented plane wave (FLAPW) calculation
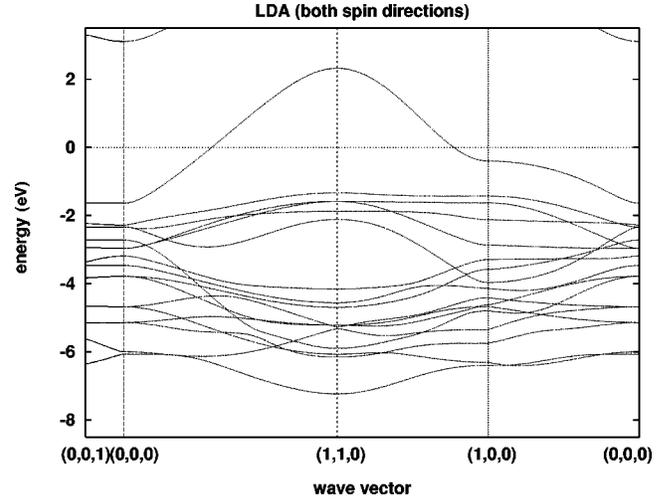
FIG. 2. The LDA-LCAO band structure of $Sr_2CuO_2Cl_2$. The wave vector is given in units of $(\pi/a,\pi/a,\pi/c)$.

has been performed for $Sr_2CuO_2Cl_2$ (Fig. 3; compare also Ref. 23). This method involves no shape approximations and uses a flexible basis in all regions of space.[24] As such it is well suited to open structures with low site symmetries as in the present cuprate. We note a sufficiently good agreement between both band structures, although the LCAO bandwidth of the valence band is found to be somewhat larger. However, there are no significant differences in the order of energy levels between LCAO-LDA and FLAPW-LDA. We stick to the LCAO because we want to exploit the minimum basis orbital analysis.

To obtain more information about the structure of the valence band in our LCAO-LDA we have calculated the orbital weight (defined in Ref. 25) of each band at the high symmetry points. Due to the low cross section of the Cl $3p$ orbitals for 35 eV photon energy we concentrate on the Cu $3d$ and O $2p$ orbitals (i.e., on 11 bands). The eigenfunctions with a dominant contribution from Cu $3d$ and O $2p$ orbitals are collected in Table I. The in-plane oxygen orbitals are divided into p_σ orbitals which are directed to the Cu site and p_π orbitals perpendicular to them.[26] There are two combinations
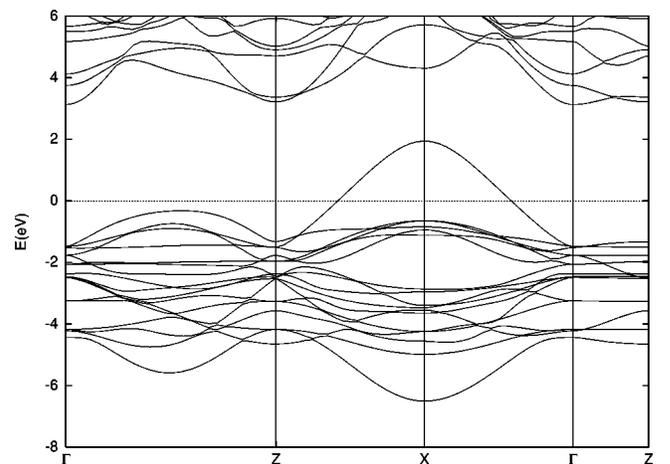
FIG. 3. The LDA-FLAPW band structure of $Sr_2CuO_2Cl_2$. The points in k space are denoted as $Z=(0,0,\pi/c)$ and $X=(\pi/a,\pi/a,0)$.

TABLE I. LDA data at high symmetry points showing the weights of the different orbital groups contributing to each band. Also given are the different reflection symmetries with respect to M_1 and M_2, respectively [antisymmetric (A), symmetric (S), and out-of-plane bands (o)].

Γ

No.	E/eV	p_z	p_σ	p_π	$d_{3z^2-r^2}$	$d_{(x,y)z}$	d_{xy}	$d_{x^2-y^2}$	O_s	Cu_s	ΣCl	Not.	M_1	M_2
1	−1.64	0	0	0	0	0	0	0.903	0.097	0	0	$d_{x^2-y^2}$	A	S
2	−2.28	0	0	0	0.817	0	0	0	0.015	0.005	0.163	$d_{3z^2-r^2}$	S	S
3,4	−2.34	0	0.456	0.530	0	0	0	0	0	0	0.014	$(p_\pi p_\sigma)$	A	S
												$(\tilde{p}_\pi \tilde{p}_\sigma)$	S	A
5	−2.72	0	0	0	0	0	1.00	0	0	0	0	d_{xy}	S	A
6,7	−2.96	0	0	0	0	0.984	0	0	0	0	0.016	$d_{(x,y)z}$	o	o
8,9	−3.46	1.00	0	0	0	0	0	0	0	0	0	p_z	o	o
	(−3.19)	(0.526)									(0.474)			
10,11	−5.14	0	0.495	0.495	0	0	0	0	0	0	0.010	$(p_\sigma p_\pi)$	A	S
												$(\tilde{p}_\sigma \tilde{p}_\pi)$	S	A

(π,π)

No.	E/eV	p_z	p_σ	p_π	$d_{3z^2-r^2}$	$d_{(x,y)z}$	d_{xy}	$d_{x^2-y^2}$	Cu_s	O_s	ΣCl	Not.	M_1
1	2.32	0	0.554	0	0	0	0	0.446	0	0	0	$(d_{x^2-y^2} p_\sigma)$	A
2	−1.33	0	0	0.196	0.006	0	0.792	0	0	0	0.006	$(d_{xy}\tilde{p}_\pi)$	S
3,4	−1.58	0.563	0	0	0	0.437	0	0	0	0	0	$(d_{(x,y)z} p_z)$	o
5	−1.87	0	0.038	0	0.637	0	0.009	0	0.055	0	0.261	$(d_{3z^2-r^2}\tilde{p}_\sigma)$	S
6	−2.12	0	0	1.00	0	0	0	0	0	0	0	p_π	A
7,8	−4.56	0.641	0	0	0	0.268	0	0	0	0	0.091	$(p_z d_{(x,y)z})$	o
9	−5.21	0	0.424	0	0	0	0	0.576	0	0	0	$(p_\sigma d_{x^2-y^2})$	A
10	−6.15	0	0.003	0.702	0.001	0	0.291	0	0	0	0.003	$(\tilde{p}_\pi d_{xy})$	S
11	−7.23	0	0.495	0	0.018	0	0	0	0.294	0	0.193	$(\tilde{p}_\sigma d_{3z^2-r^2})$	S

(π,0)

No.	E/eV	p_z	p_σ	p_π	$d_{3z^2-r^2}$	d_{yz}	d_{xz}	d_{xy}	$d_{x^2-y^2}$	Cu_s	O_s	ΣCl	Not.	M_2
1	−0.40	0	0.128	0	0.015	0	0	0	0.599	0.105	0.105	0.049	$(d_{x^2-y^2} p_\sigma)$	S
2	−1.42	0	0	0.335	0	0	0	0.665	0	0	0	0	$(d_{xy}\tilde{p}_\pi)$	A
3	−1.63	0.395	0	0	0	0	0.601	0	0	0	0	0.004	$(d_{xz} p_z)$	o
4	−2.12	0	0.002	0.001	0.655	0	0	0	0.096	0.007	0.019	0.220	$(d_{3z^2-r^2} d_{x^2-y^2})$	S
5	−2.87	0	0	0	0	0.880	0	0	0	0	0	0.120	d_{yz}	o
6	−3.29	0.594	0	0	0	0	0.019	0	0	0	0	0.387	p_z	o
7	−3.58	0	0.532	0	0	0	0	0	0	0	0	0.468	$\tilde{p}_\sigma$	A
8	−3.96	0	0	0.935	0	0	0	0	0	0	0.046	0.019	p_π	S
9	−4.13	0.403	0	0	0	0	0.270	0	0	0	0	0.327	$(p_z d_{xz})$	o
10	−4.62	0	0.057	0.475	0	0	0	0	0.348	0	0	0.120	$(\tilde{p}_\pi d_{xy})$	A
11	−5.74	0	0.268	0.004	0.079	0	0	0	0.149	0.032	0.009	0.459	$(p_\sigma d_{x^2-y^2})$	S

for each: p_σ and $\tilde{p}_\sigma$, (p_π and $\tilde{p}_\pi$), which are antisymmetric and symmetric with respect to reflection in M_1, respectively. The precise definition of these orbitals will be given in the next section.

Thus we are able to predict the symmetry of each band at the high symmetry points in the Brillouin zone (BZ). However, as will be seen later, the order of energy levels of the LDA calculation is incompatible with the experimental spectra. Moreover, as it was mentioned already, LDA calculations are unable to describe the Mott insulating ground states of the undoped cuprates and do not produce the Cu local moments that are present in these systems. The splitting of the spectral density due to the $3d_{x^2-y^2}$ states away from the

Fermi energy due to Coulomb correlations and the resulting reduction in Cu-O hybridization is expected to be largely missing in such calculations. However, what, if any, changes there are from the LDA bands away from E_F is unclear, particularly well above T_N, where the magnetic scattering due to antiferromagnetic spin fluctuations should be more or less incoherent. Addressing this question is one of the main goals of the present paper. In the following we develop a more sophisticated LDA+U calculation taking into account explicitly the effects of strong correlations. As a preliminary step we formulate an effective tight-binding model which will be fitted both to the LDA+U band structure calculations and the ARPES VB spectra.
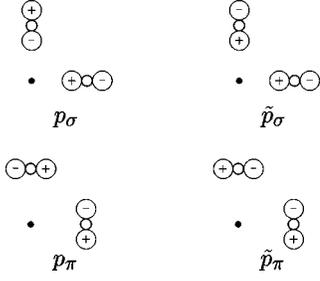
FIG. 4. Sketch of the different oxygen orbitals within one unit cell (filled circles: copper; open circles: oxygen) for momenta $q \rightarrow 0$ along $\Gamma - (\pi, \pi)$.

IV. SYMMETRY ANALYSIS AND TIGHT-BINDING MODEL

The polarization dependent ARPES measurements of VB states along the two high-symmetry directions $\Gamma - (\pi, \pi)$ and $\Gamma - (\pi, 0)$ discriminate the parity of these states with respect to reflections in the corresponding mirror planes M_1 and M_2. To make the analysis of the experimental data more straightforward it is helpful to incorporate the symmetry properties of the VB states in our approach from the beginning. This becomes especially clear by constructing an effective tight-binding (TB) model taking into account the point-group symmetry of the VB states. The TB model will be restricted to the 11 bands of Cu $3d$ and O $2p$. Of course, as can be seen in Table I, there occurs in some cases quite a strong mixing with the Cl subsystem, but in the following we will assume that this mixing is taken into account by the particular values of the TB parameters.

We start with the description of in-plane oxygen orbitals whose analysis is more involved than that for the copper or out-of-plane orbitals. We introduce the annihilation operator of an electron in the two oxygen π orbitals belonging to an elementary cell at position $\vec{i}$ ($\vec{i}$ is a site of the square lattice) as $p_{\vec{i}+\vec{\beta}/2}^{(\alpha)}$, where $(\vec{\alpha}, \vec{\beta}) = (\vec{x}, \vec{y})$ or $(\vec{y}, \vec{x})$ with $\vec{x}$ and $\vec{y}$ to be the two orthogonal unit vectors of the lattice. The d_{xy} orbitals hybridize with a particular combination of oxygen orbitals arranged over the plaquette at site $\vec{i}$: $p_{\pi i} = \frac{1}{2}(p_{\vec{i}+\vec{x}/2}^{(y)} - p_{\vec{i}-\vec{x}/2}^{(y)} + p_{\vec{i}+\vec{y}/2}^{(x)} - p_{\vec{i}-\vec{y}/2}^{(x)})$. This plaquette's π orbitals are not orthogonal to each other. The orthogonalization can be made by introducing first the Fourier transformation for the original p_{π} orbitals

$$p_{\pi}^{(\alpha)}(q) = \frac{1}{\sqrt{N}} \sum_{i} p_{\vec{i}+\vec{\beta}/2}^{(\alpha)} e^{-i\vec{q}(\vec{i}+\vec{\beta}/2)}.$$

At the second step we define two kinds of canonical Fermi operators

$$p_{\pi}(q) = \lambda_q^{-1} i (s_{q,y} p_{\pi}^{(y)}(q) - s_{q,x} p_{\pi}^{(x)}(q)),$$

$$\tilde{p}_{\pi}(q) = \lambda_q^{-1} i (s_{q,x} p_{\pi}^{(y)}(q) + s_{q,y} p_{\pi}^{(x)}(q)), \quad (1)$$

where $s_{q,\alpha} = \sin(q_\alpha/2)$ ($\alpha = x, y$) and $\lambda_q = \sqrt{s_{q,x}^2 + s_{q,y}^2}$. It is easy to see that p_{π} and $\tilde{p}_{\pi}$ are orthogonal with respect to each other. The definition (1) provides an equivalent representation for π orbitals in terms of $p_{\pi}(q)$ and $\tilde{p}_{\pi}(q)$, instead of the original $p_{\pi}^{(x)}(q)$ and $p_{\pi}^{(y)}(q)$ operators and takes into

account the point group symmetry of the CuO$_2$ plane. In particular, for q along $\Gamma - (\pi, \pi)$, the p_{π} orbital is antisymmetric with respect to reflections in the mirror plane M_1, while the $\tilde{p}_{\pi}$-orbital is symmetric (see Fig. 4). Along $\Gamma - (\pi, 0)$, we find p_{π} to be symmetric and $\tilde{p}_{\pi}$ to be antisymmetric with respect to reflection in M_2.

Turning now to the oxygen σ orbitals we carry out the same procedure as above with the corresponding $p_{\vec{i}+\alpha/2}^{(\alpha)}$ operators ($\vec{\alpha} = \vec{x}, \vec{y}$). In this case, introducing the plaquette representation instead of defining the original $p_{\sigma}^{(\alpha)}$ operators in momentum space, we define a new pair of canonical Fermi operators p_{σ} and $\tilde{p}_{\sigma}$:

$$p_{\sigma}(q) = \lambda_q^{-1} i (s_{q,x} p_{\sigma}^{(x)}(q) - s_{q,y} p_{\sigma}^{(y)}(q)),$$

$$\tilde{p}_{\sigma}(q) = \lambda_q^{-1} i (s_{q,y} p_{\sigma}^{(x)}(q) + s_{q,x} p_{\sigma}^{(y)}(q)).$$

The notation is chosen in such a way that the $p_{\sigma}(q) [\tilde{p}_{\sigma}(q)]$ orbitals have the same symmetry properties with respect to reflections at M_1 and M_2 as the $p_{\pi}(q)$ or $\tilde{p}_{\pi}(q)$ orbitals, respectively.

The definition of the corresponding copper annihilation operators is quite standard and thus we may write down the TB Hamiltonian

$$H_t = \sum_{q\mu\nu s} c_{\mu s}^{\dagger}(q) H_{\mu\nu}(q) c_{\nu s}(q). \quad (2)$$

Here, $c_{\mu s}$ is an annihilation operator of either an oxygen p orbital or a copper d orbital, where the indices μ and ν denote the 11 different orbitals and s denotes the spin. All orbitals can be classified as to whether they hybridize in-plane or out-of-plane and there is no coupling between the two subsystems. The orbitals involved in the hybridization in-plane are p_{σ}, p_{π}, $\tilde{p}_{\sigma}$, $\tilde{p}_{\pi}$, $d_{x^2-y^2}$, d_{xy}, $d_{3z^2-r^2}$. The explicit form of the TB Hamiltonian for in-plane orbitals is given in the Appendix. The in-plane part of the TB model has 11 parameters: the on-site energies ε_d (for $d_{x^2-y^2}$), ε_D (for d_{xy}) and $\varepsilon_{\tilde{d}}$ (for $d_{3z^2-r^2}$) as well as ε_p (corresponding to p_{σ}) and ε_{π}; the hopping matrix elements t_{pd}, t_{pD}, $t_{p\tilde{d}}$, t_{pp}, $t_{\pi\pi}$, and $t_{p\pi}$. Besides the orbitals hybridizing in-plane we have to consider those involved in hybridization out-of-plane: O $2p_z$, Cu $3d_{xz}$, and Cu $3d_{yz}$. Restricting ourselves to nearest neighbor hopping leads to two 2×2 matrices with on-site energies ε_{pz} and ε_{dz} and the hopping matrix element t_{pdz}.

In order to analyze the experiment it is important to know the parity of the orbitals with respect to reflections at the corresponding mirror planes M_1 and M_2. This can also be expressed in terms of group theory since for k vectors along the line $\Gamma - (\pi, \pi)$ all wave functions can be classified in terms of irreducible representations of the small group C_{2v}.[27–29] The bands built up from the in-plane orbitals d_{xy}, $d_{3z^2-r^2}$, $\tilde{p}_{\sigma}$, and $\tilde{p}_{\pi}$ belong to the representation A_1 and are symmetric with respect to reflections at M_1, whereas $d_{x^2-y^2}$, p_{σ} and p_{π} belong to A_2 and are antisymmetric. The same small group C_{2v} also acts along $\Gamma - (\pi, 0)$ and the subdivision of the in-plane orbitals is as follows: A_1 (symmetric): $d_{x^2-y^2}$, $d_{3z^2-r^2}$, p_{σ}, p_{π} and A_2 (antisymmetric): d_{xy}, $\tilde{p}_{\sigma}$,

TABLE II. Assignment of the orbitals to irreducible representations of the corresponding small groups at high symmetry points: (a) Γ (group D_{4h}), (b) (π,π) (D_{4h}), and (c) $(\pi,0)$ (D_{2h}). The notations in parentheses are according to Luehrmann (Ref. 28) (see also Ref. 26). Also given are the characters with respect to reflections at M_1 or M_2, respectively, whereby $+$ and $-$ correspond to the S and A given in Table I. The orbital $p_z^{(1)}$ means p_z orbitals at positions $i\pm x/2$, and $p_z^{(2)}$ at positions $i\pm y/2$.

(a) Γ

Orbitals	Repr.		M_1	M_2
p_σ, $\tilde{p}_\sigma$	$E_u^{(1)}$	(5^-)	0	0
p_π, $\tilde{p}_\pi$	$E_u^{(2)}$	(5^-)	0	0
$(p_z^{(1)}+p_z^{(2)})/\sqrt{2}$	A_{2u}	(2^-)	$+$	$+$
$(p_z^{(1)}-p_z^{(2)})/\sqrt{2}$	B_{2u}	(4^-)	$-$	$+$
$d_{x^2-y^2}$	B_{1g}	(3^+)	$-$	$+$
d_{xy}	B_{2g}	(4^+)	$+$	$-$
$d_{(x,y)z}$	E_g	(5^+)	0	0
$d_{3z^2-r^2}$	A_{1g}	(1^+)	$+$	$+$

(b) (π,π)

Orbitals	Repr.		M_1
$d_{3z^2-r^2}$, $\tilde{p}_\sigma$	A_{1g}	(1^+)	$+$
p_π	A_{2g}	(2^+)	$-$
$d_{x^2-y^2}$, p_σ	B_{1g}	(3^+)	$-$
d_{xy}, $\tilde{p}_\pi$	B_{2g}	(4^+)	$+$
$d_{(x,y)z}$, $p_z^{(1,2)}$	E_g	(5^+)	0

(c) $(\pi,0)$

Orbitals	Repr.		M_1
$d_{x^2-y^2}$, $d_{3z^2-r^2}$, p_σ	A_g	(1^+)	$+$
d_{xy}, $\tilde{p}_\pi$	B_{1g}	(2^+)	$-$
$\tilde{p}_\sigma$	B_{2u}	(3^-)	$-$
p_π	B_{3u}	(4^-)	$+$
d_{xz}, $p_z^{(1)}$	B_{2g}	(3^+)	$+$
$p_z^{(2)}$	B_{1u}	(2^-)	$+$
d_{yz}	B_{3g}	(4^+)	$+$

$\tilde{p}_\pi$. The subdivision along high-symmetry lines is also easily seen in the TB matrix given in the Appendix. The corresponding small groups at the high-symmetry points Γ, (π,π) and $(\pi,0)$ are D_{4h} and D_{2h}, respectively, and the assignment of the different orbitals to the corresponding irreducible representations is given in Table II. Of course, the group theoretical analysis is not only valid for the TB model but also for the LDA bands (Table I).

The TB Hamiltonian (2) should be completed by an interaction term

$$H=H_t+H_U, \qquad (3)$$

which will not be written out explicitly. This is just a direct extension of the three-band Emery model to the case of the complete set of 11 bands for the CuO_2 plane. The interaction term H_U involves intrasite Hubbard repulsion for different kinds of copper and oxygen orbitals and appropriate intersite copper-oxygen repulsions. In order to establish the one-

electron parameters entering into Eq. (3) one has to keep in mind that these parameters are ''bare'' ones while the results of the band structure calculations should be interpreted in terms of a mean-field solution of Eq. (3).[30] To arrive at the bare parameters, one would have to take into account the ground-state (G.S.) properties of the CuO_2 plane and approximate the Coulomb interaction terms.

In an undoped cuprate compound as $Sr_2CuO_2Cl_2$, the G.S. of a particular CuO_2 plane contains one hole per cell which is shared between $d_{x^2-y^2}$ and p_σ orbitals. Thus a convenient description of the G.S. is to introduce the deviations $\langle n_s^d\rangle_h=1-\langle n_s^d\rangle$ and $\langle n_s^p\rangle_h=1-\langle n_s^p\rangle$ from the full band (Cu $3d^{10}$ O $2p^6$) electron occupancy. A rough estimate is $\langle n_s^d\rangle_h \approx 0.7$ and $\langle n_s^p\rangle_h\approx 0.3$. Here $\langle n_s^p\rangle$ means the electron number in the p_σ orbital with spin s (one should note that the occupation of a local oxygen orbital is only half that number). Now the mean-field (''screened'') one-electron energies $\bar{\varepsilon}_{\mu s}$ read as follows:

$$\bar{\varepsilon}_{ds}=\varepsilon_d+U_d-U_d\langle n_{\bar{s}}^d\rangle_h-2U_{pd}\left\langle \sum_{s'} n_{s'}^p\right\rangle_h,$$

$$\bar{\varepsilon}_{ps}=\varepsilon_p+U_p-2U_{pd}\left\langle \sum_{s'} n_{s'}^d\right\rangle_h-\frac{1}{2}U_p\langle n_{\bar{s}}^p\rangle_h,$$

$$\bar{\varepsilon}_D=\varepsilon_D+U_d-U_{dD}\left\langle \sum_{s'} n_{s'}^d\right\rangle_h-2U_{Dp}\left\langle \sum_{s'} n_{s'}^p\right\rangle_h,$$

$$\bar{\varepsilon}_\pi=\varepsilon_p+U_\pi-\frac{1}{2}U_{p\pi}\left\langle \sum_{s'} n_{s'}^p\right\rangle_h-2U_{d\pi}\left\langle \sum_{s'} n_{s'}^d\right\rangle_h,$$

$$(4)$$

where $\bar{s}=-s$. There are also similar expressions for $\bar{\varepsilon}_{\tilde{d}}$, $\bar{\varepsilon}_{dz}$, $\bar{\varepsilon}_{pz}$ which we do not specify here.

In the paramagnetic LDA band structure where the correlation effects are treated only in an averaged manner, the screening effect is nearly the same for all d levels. So, in the LDA approach the effects of strong correlations due to U_d are missed. An obvious way to adopt these effects is to treat the ferromagnetic solution by putting, for instance, $\langle n_\downarrow^d\rangle_h=0$, and $\langle n_\uparrow^d\rangle_h=n^d$. Then $\bar{\varepsilon}_{d\uparrow}=\varepsilon_d+U_d-2U_{pd}n^p$ ($n^p=\Sigma_s\langle n_s^p\rangle_h$), is shifted upwards while $\bar{\varepsilon}_{d\downarrow}=\varepsilon_d+U_d(1-n^d)-2U_{pd}n^p$ is shifted equally downwards with respect to the paramagnetic solution. Regarding the other d levels, let us assume for the moment the rough estimate for the intrasite Coulomb parameters $U_{dD}\simeq U_d$. Then one can see that $\bar{\varepsilon}_D=\varepsilon_D+U_d(1-n^d)-2U_{pd}n^p$, and the d_{xy} level as well as all the other remaining Cu d levels are shifted as was the lower $\bar{\varepsilon}_{d\downarrow}$. The spin dependence of $\bar{\varepsilon}_{ps}$ in Eq. (4) is much less pronounced than for $\bar{\varepsilon}_{ds}$ and is neglected in the following.

Thus, although being somewhat awkward, the ferromagnetic solution provides a better description of the strong electron correlations, giving a more reasonable energy position and occupancy of the different orbitals. Just this approach is taken by us to carry out the LDA+U calculation. The details of the procedure and some results of these calculation are presented in the next section.
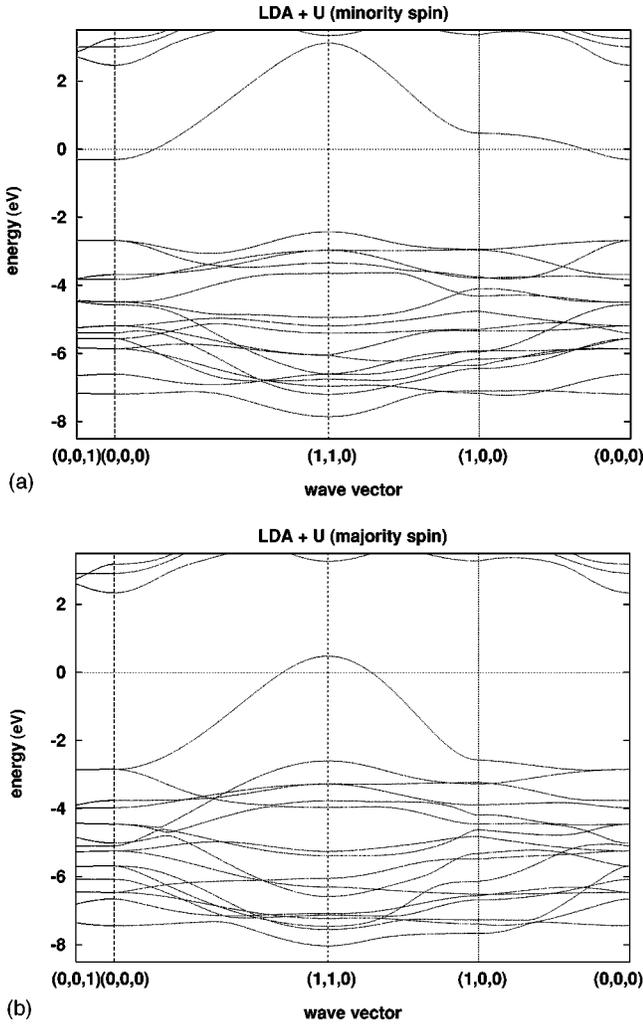
FIG. 5. LDA+U band structure: (a) minority spin ($\uparrow$); (b) majority spin ($\downarrow$).

V. LDA+U CALCULATION

The main effect of a mean-field treatment of the multiband Hubbard model is a shift of the on-site copper energies against the oxygen ones. Furthermore, the on-site energy of the Cu $3d_{x^2-y^2}$ orbital is split into one for spin up $\bar{\varepsilon}_{d\uparrow}$ (minority spin) and $\bar{\varepsilon}_{d\downarrow}$ (majority spin). This can also be achieved by an LDA+U calculation[16] including all valence orbitals.

We performed LDA+U calculations for $Sr_2CuO_2Cl_2$ using a ferromagnetic splitting. The on-site energy of the unoccupied, spin up Cu $3d^{\uparrow}_{x^2-y^2}$ orbital (minority spin) is shifted by 2 eV upwards and the occupied, spin down Cu $3d^{\downarrow}_{x^2-y^2}$ orbital (majority spin), as well as both spin directions for all the remaining Cu $3d$ orbitals are shifted by 2 eV downwards. The energy shifts were added at each step of the self-consistency cycle until the charge distribution was stable. We did not try to connect the chosen energy shifts with the model parameters such as, for instance, U_d, U_{pd}, U_p. According to Eq. (4), the actual shift depends also on the occupation numbers $\langle n^d_s \rangle_h$ and $\langle n^p_s \rangle_h$. Since we did not shift the oxygen levels, our choice corresponds in fact to the difference between U_d and U_p weighted with the corresponding occupation numbers.

The results of our LDA+U calculation are presented in Fig. 5 and Table III. The mainly unoccupied, minority band of $d_{x^2-y^2}$ and p_σ character can be roughly interpreted as the upper Hubbard band. The corresponding band for majority spin lies just below the Fermi level and has dominantly oxygen character. Since its spin is opposite to the spin of the copper hole, there is some justification to interpret that band as the mean field representation of the Zhang-Rice singlet. But due to our ferromagnetic spin structure it has completely the wrong dispersion relation.[31] The bandwidth of both bands is expected to be strongly reduced by correlation effects in comparison with Fig. 5 such that a gap opens.

Next in binding energy we find bands with dominantly oxygen character. The nonbonding oxygen band with lowest binding energy at (π,π) is identified to be of pure p_π character. The oxygen bands occur at nearly the same energy for both spin directions. In fact, only the bands with a considerable weight of the Cu $3d_{x^2-y^2}$ orbital show a strong splitting between spin up and spin down. Therefore we present in Table III only the position of minority spin bands and both spin directions for bands with a contribution from the $3d_{x^2-y^2}$ orbital.[32] The actual value of the energy shifts of the copper bands in our LDA+U calculation has little influence on the upper oxygen bands, only their copper character is changed. We have chosen such a shift that the copper bands are at the lower edge of the valence band, but are not yet split off the valence band. This is important in order to achieve good agreement with the experimental results.

Let us now compare the LDA and LDA+U results starting at (π,π). In both cases (Figs. 2 and 5), we find a group of 5 bands at around 3 eV binding energy, but the order of energy levels is completely different in the two cases. For example, the antisymmetric p_π band has lowest binding energy of ≈ 2.5 eV in the LDA+U calculation. In Fig. 2 (LCAO-LDA), however, all the other 4 bands of that group have lower binding energy than the p_π level. And also in the FLAPW calculation (Fig. 3) the p_π band has 0.3 eV larger binding energy than the valence band edge. A similar rearrangement of energy levels can be observed at the Γ point. Due to symmetry reasons there is no hybridization between copper and oxygen bands there. The energy position of the oxygen bands is nearly the same for LDA and LDA+U, but the copper bands are shifted. The in-plane oxygen bands are twofold degenerate and occur twice in the LDA+U result with binding energies of 2.69 and 5.57 eV, respectively.

VI. COMPARISON WITH EXPERIMENT

A. High-symmetry points

The experimental ARPES spectra at the high symmetry points for both polarization directions are presented in Fig. 6. At the Γ point, there are two possible orientations of the sample such that one can probe the symmetry of states with respect to reflections in either M_1 [sample directed such that the photoelectron momentum is along $\Gamma-(\pi,\pi)$, Fig. 6(a)], or M_2 [sample directed such that the photoelectron momentum is along $\Gamma-(\pi,0)$, Fig. 6(b)]. The first peak at 2.9 eV binding energy in the experimental spectra at the Γ point with the sample oriented such that the k vector is along $\Gamma-(\pi,\pi)$ [Fig. 6(a)] is equally strong for both polarization directions. This leads us to interpret it as the two pure oxy-

TABLE III. The LDA+U data at the high symmetry points. The bands noted by a star correspond to majority spin ($\downarrow$), whereas all the other data are given for minority spin ($\uparrow$). The column ''Not.'' gives the notation used to describe the bands.

Γ

No.	E/eV	p_z	p_σ	p_π	$d_{3z^2-r^2}$	d_{yz}	d_{xz}	d_{xy}	$d_{x^2-y^2}$	O_s	Cu_s	ΣCl	Not.	M_1	M_2
1	−0.30	0	0	0	0	0	0	0	0.909	0.091	0	0	$d^\uparrow_{x^2-y^2}$	A	S
2,3	−2.69	0	0.439	0.543	0	0	0	0	0	0	0	0.018	$(\tilde{p}_\pi\tilde{p}_\sigma)$	S	A
													$(p_\pi p_\sigma)$	A	S
4,5	−3.83 (−3.69)	1.00 (0.567)	0	0	0	0	0	0	0	0	0	0 (0.433)	p_z	o	o
6	−4.58	0	0	0	0.640	0	0	0	0	0.031	0	.329	$d_{3z^2-r^2}$	S	S
7*	−4.92	0	0	0	0	0	0	0	0.893	0.107	0	0	$d^\downarrow_{x^2-y^2}$	A	S
8	−5.40	0	0	0	0	0	0	1.00	0	0	0	0	d_{xy}	S	A
9,10	−5.57	0	0.499	0.463	0	0	0	0	0	0	0	0.038	$(\tilde{p}_\sigma\tilde{p}_\pi)$	S	A
													$(p_\pi p_\sigma)$	A	S
11,12	−5.88	0	0	0	0	0.803	(0.803)	0	0	0	0	0.197	$d_{y(x)z}$	o	o

(π,π)

No.	E/eV	p_z	p_σ	p_π	$d_{3z^2-r^2}$	d_{yz}	d_{xz}	d_{xy}	$d_{x^2-y^2}$	O_s	Cu_s	ΣCl	Not.	M_2
1	3.12	0	0.467	0	0	0	0	0	0.533	0	0	0	$(d^\uparrow_{x^2-y^2}p_\sigma)$	A
2*	0.65	0	0.704	0	0	0	0	0	0.296	0	0	0	$(p_\sigma d^\downarrow_{x^2-y^2})$	A
3	−2.43	0	0	1.00	0	0	0	0	0	0	0	0	p_π	A
4,5	−2.98 (−2.97)	0.711	0	0	0	0.143	0.143	0	0	0	0	0.002 (.006)	$(p_z d_{x(y)z})$	o
6	−3.35	0	0.009	0.345	0.030	0	0	0.564	0	0	0.004	0.048	$(\tilde{p}_\pi d_{xy})$	S
7	−3.66	0	0.096	0.020	0.356	0	0	0.053	0	0	0.051	0.424	$(d_{3z^2-r^2}p_\sigma)$	S
8	−4.94	0	0.561	0	0	0	0	0	0.439	0	0	0	$(p_\sigma d^\uparrow_{x^2-y^2})$	A
9,10	−6.62 (−6.06)	0.155 (0.093)	0	0	0	0.341 (0.275)	0.341 (0.275)	0	0	0	0	0.123 (0.357)	$(d_{x(y)z}p_z)$	o
11	−7.20	0	0.003	0.392	0.010	0	0	0.591	0	0	0	0.004	$(d_{xy}\tilde{p}_\pi)$	S
12*	−7.28	0	0.207	0	0	0	0	0	0.793	0	0	0	$d^\downarrow_{x^2-y^2}p_\sigma$	A
13	−7.86	0	0.478	0.001	0.073	0	0	0	0	0	0.280	0.168	$(\tilde{p}_\sigma d_{3z^2-r^2})$	S

$(\pi,0)$

No.	E/eV	p_z	p_σ	p_π	$d_{3z^2-r^2}$	d_{xz}	d_{yz}	d_{xy}	$d_{x^2-y^2}$	O_s	Cu_s	ΣCl	Not.	M_2
1	0.47	0	0.053	0	0	0	0	0	0.696	0.124	0.106	0.021	$(d^\uparrow_{x^2-y^2}p_\sigma)$	S
2*	−2.40	0	0.273	0	0.039	0	0	0	0.323	0.083	0.119	0.163	$(p_\sigma d^\downarrow_{x^2-y^2})$	S
3	−2.94	0	0	0.659	0	0	0	0.341	0	0	0	0	$(\tilde{p}_\pi d_{xy})$	A
4	−2.96	0.704	0	0	0	0.245	0	0	0	0	0	0.051	$(p_z d_{xz})$	o
5	−3.76	0	0.086	0.003	0.344	0	0	0	0.057	0.006	0.017	0.487	$(d_{3z^2-r^2}p_\sigma)$	S
6	−3.79	0.705	0	0	0	0.013	0	0	0	0	0	0.282	p_z	o
7	−4.11	0	0.635	0	0	0	0	0	0	0	0	0.365	$\tilde{p}_\sigma$	A
8	−4.32	0	0	0.933	0.001	0	0	0	0	0.049	0	0.017	p_π	S
9	−5.93	0	0	0	0	0	0.859	0	0	0	0	0.141	d_{yz}	o
10	−6.17	0	0	0.199	0	0	0	0.801	0	0	0	0	$(d_{xy}\tilde{p}_\pi)$	A
11	−6.37	0.128	0	0	0	0.384	0	0	0	0	0	0.488	$(d_{xz}p_z)$	o
12	−6.44	0	0.390	0	0.409	0	0	0	0.104	0.035	0.062	0	$(p_\sigma d_{3z^2-r^2})$	S
13*	−7.49	0	0.298	0	0.060	0	0	0	0.520	0.004	0.076	0.042	$(d^\downarrow_{x^2-y^2}p_\sigma)$	S

gen bands $(p_\pi p_\sigma)$ and $(\tilde{p}_\pi\tilde{p}_\sigma)$ which are antisymmetric and symmetric with respect to reflections at M_1, respectively.[33] These bands occur in the LDA+U calculation as the twofold degenerate in-plane oxygen bands at 2.69 eV binding energy. According to this interpretation we would expect the same identical peak for both spin directions also at the Γ point with the sample oriented such that the k vector is along Γ −$(\pi,0)$ [Fig. 6(b)]. As one can see, Fig. 6(b)] deviates only slightly from that expectation. In the LDA result, however, there are three copper levels between 2.3 and 3 eV binding energy. Since every copper level has different symmetry properties with respect to M_1 and M_2 that would lead to strong differences between both polarization directions which is not observed. Therefore, we assign each experimen-

Γ / Γ -- (π,π)

Normalized intensity (arb. units)

1 $(p_\pi p_\sigma)$
2 $(\tilde{p}_\pi \tilde{p}_\sigma)$
3 p_z
4 d_{xy}
  $(\tilde{p}_\sigma \tilde{p}_\pi)$
5 $d^\downarrow_{x^2-y^2}$
  $(p_\sigma p_\pi)$
6 $d_{(x,y)z}$

(a)   Binding energy (eV)

(π,π) / Γ -- (π,π) M₁

Normalized intensity (arb. units)

1 $(p_\sigma d^\downarrow_{x^2-y^2})$
2 p_π
3 $(p_z d_{(x,y)z})$
  $(\tilde{p}_\pi d_{xy})$
4 $(p_\sigma d^\uparrow_{x^2-y^2})$
5 $(d_{(x,y)z} p_z)$
  $(d_{xy} \tilde{p}_\pi)$
6 $(d^\downarrow_{x^2-y^2} p_\sigma)$

(c)   Binding energy(eV)

Γ / Γ -- (π,0)

Normalized intensity (arb. units)

1 $(\tilde{p}_\pi \tilde{p}_\sigma)$
2 $(p_\pi p_\sigma)$
3 p_z
4 $(d^\downarrow_{x^2-y^2})$
  $(p_\sigma p_\pi)$
5 d_{xy}
  $(\tilde{p}_\sigma \tilde{p}_\pi)$
6 $d_{(x,y)z}$

(b)   Binding energy (eV)

(π,0) / Γ -- (π,0) M₂

Normalized intensity (arb. units)

1 $(p_\sigma d^\downarrow_{x^2-y^2})$
2 $(p_z d_{xz})$
3 $(\tilde{p}_\pi d_{xy})$
4 p_z
  p_π
5 $\tilde{p}_\sigma$
6 $(d_{xy} \tilde{p}_\pi)$
7 d_{yz}
  $(d_{xz} p_z)$

(d)   Binding energy (eV)

FIG. 6. Experimental photoemission data at high-symmetry points, with the relevant mirror plane given in brackets: (a) at the Γ point (M_1), (b) at the Γ point (M_2), (c) at (π,π) (M_1), and (d) $(\pi,0)$ (M_2). The assignment of peaks is according to the LDA+U results. The filled circles and full lines correspond to vertical polarization, whereas the open circles and broken lines give the results for horizontal polarization.

tal peak with the help of the LDA+U results. Each pure band is denoted by one orbital only. For the mixed bands we choose a notation using two orbitals, where the first one is the dominant one. The experimental peak positions are compared with the LDA+U positions in Table IV.

Let us continue our interpretation of the spectra at the Γ point with the peak at 3.9 eV. It is seen with horizontal polarization in Figs. 6(a) and 6(b). Therefore, we interpret it as the out-of-plane oxygen p_z orbital. We observe also a small contribution of this peak with the "wrong" polarization in Fig. 6(a) which is even larger in Fig. 6(b). However, there is no band with the corresponding symmetry in that energy region in our LDA+U calculation. The large peaks at around 6 eV binding energy in Figs. 6(a) and 6(b) with big differences between both polarization directions indicate that there are additional contributions besides the oxygen orbitals there. Due to the low cross section of Cl $3p$ orbitals, we are only left with the pure copper d orbitals. To simplify the analysis we did not try to assign the Cu $3d_{3z^2-r^2}$ orbital

which mixes strongly with the Cl orbitals and should have reduced intensity. The remaining in-plane copper orbitals change their polarization dependence between Figs. 6(a) and 6(b). The $d^\downarrow_{x^2-y^2}$ is antisymmetric with respect to M_1 and the d_{xy} is symmetric, but with the sample oriented such that the k-vector is along $\Gamma-(\pi,0)$ this situation is reversed. The intensity ratio between horizontal and vertical polarization of the peak at 5.8 eV is indeed exchanged if we compare Figs. 6(a) and 6(b). The last peak at 6.5 eV occurs for both sample orientations only with horizontal polarization and is interpreted as the out-of-plane d_{xz} or d_{yz} orbital.

Turning now to the spectra at (π,π) we can only probe the parity with respect to M_1 [Fig. 6(c)]. The small prepeak at 1.2 eV in the curve with vertical polarization is ususally interpreted as the Zhang-Rice singlet.[2] The dominant peak at 2.4 eV binding energy in the spectra with perpendicular polarization can be identified as the pure p_π orbital which has already been discussed in Ref. 10. The p_π band is the only one among the group of 5 bands at around 3 eV binding

TABLE IV. Comparison of experimental peak positions (in eV) with the LDA+U results at the high-symmetry points (ZRS and ZRT mean the Zhang-Rice singlet or triplet, respectively).

Γ		
Orbital	LDA+U	Expt.
$(p_\pi p_\sigma)$	-2.69	-2.9
$(\tilde{p}_\pi \tilde{p}_\sigma)$		
p_z	-3.83	-3.9
$d^\downarrow_{x^2-y^2}$	-4.92	-5.8
d_{xy}	-5.40	
$(p_\sigma p_\pi)$	-5.57	
$(\tilde{p}_\sigma \tilde{p}_\pi)$		
$d_{(x,y)z}$	-5.87	-6.5

(π,π)		
Orbital	LDA+U	Expt.
$(p_\sigma d^\downarrow_{x^2-y^2})$ (ZRS)	0.65	-1.2
p_π	-2.43	-2.4
$(p_z d_{(x,y)z})$	-2.98	-2.7
$(\tilde{p}_\pi d_{xy})$	-3.35	
$(p_\sigma d^\uparrow_{x^2-y^2})$ (ZRT)	-4.94	-3.8
$(d_{(x,y)z} p_z)$	-6.62	-5.8
$(d_{xy} \tilde{p}_\pi)$	-7.20	
$(d^\downarrow_{x^2-y^2} p_\sigma)$	-7.28	-6.0

$(\pi,0)$		
Orbital	LDA+U	Expt.
$(p_\sigma d^\downarrow_{x^2-y^2})$ (ZRS)	-2.40	-1.1
$(p_z d_{xz})$	-2.96	-2.5
$(\tilde{p}_\pi d_{xy})$	-2.94	-2.7
p_z	-3.79	-3.8
p_π	-4.32	
$\tilde{p}_\sigma$	-4.11	-3.8
$(d_{xy} \tilde{p}_\pi)$	-6.17	-5.6
d_{yz}	-5.93	-6.6
$(d_{xz} p_z)$	-6.37	

energy in both calculations (LDA or LDA+U, Figs. 2 and 5) which has odd symmetry with respect to M_1. It has lowest binding energy in the experiment and in the LDA+U calculation. That indicates that the LDA+U calculation is better in predicting the correct order of energy levels at high symmetry points than the pure LDA calculation. At slightly higher binding energy at 2.7 eV we observe a smaller, broader peak with horizontal polarization. According to our calculation it should be comprised of three bands, the out-of-plane $(p_z d_{(x,y)z})$ bands and the in-plane $(\tilde{p}_\pi d_{xy})$ band. The small structure at 3.8 eV binding energy (vertical polarization) can be related to the oxygen p_σ orbital hybridizing with $d_{x^2-y^2}$ but having the same spin ($\uparrow$) as that of the copper hole. The corresponding band occurs in the LDA+U at 4.94 eV binding energy and can be interpreted as the Zhang-Rice triplet. A similar structure was also observed in our previous analysis of the polarization dependent photoemission spectra of another undoped model cuprate $Ba_2Cu_3O_4Cl_2$.[13]
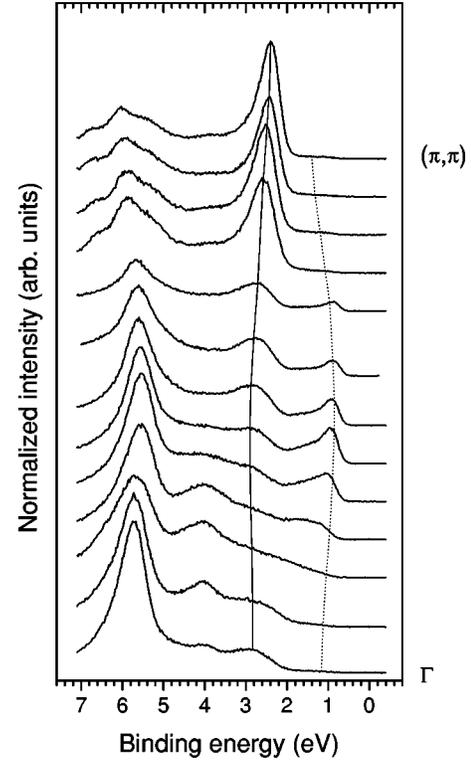
FIG. 7. Angle resolved photoemission curves along $\Gamma-(\pi,\pi)$ for vertical polarization. Also shown is the antisymmetric TB band with dominant oxygen (p_π) contribution (full line) and the dispersion of the Zhang-Rice singlet according to Ref. 9 (dotted line).

The peaks at around 6 eV binding energy should be assigned to bands with a dominant copper character. But one may note in Table IV a systematic deviation between experimental and theoretical peak positions at (π,π): the theoretical binding energies are too large. That is plausible since it is expected that the copper bands feel the antiferromagnetic correlations much more than the oxygen bands which are decoupled from the copper spins. As a result the copper bands are expected to follow more the AFM BZ where Γ and (π,π) are identical. However, such AFM correlations were not considered in our calculation.

At $(\pi,0)$ [Fig. 6(d)] one may observe a prepeak with low intensity which may be prescribed to the Zhang-Rice singlet state comprised in our calculation by the hybridization between the p_σ orbital and $d^\downarrow_{x^2-y^2}$. The strong peak with horizontal polarization at 2.5 eV is assigned to the out-of-plane $(p_z d_{xz})$ orbital. The peak at 3.8 eV consists of two orbitals p_z and p_π which are separated by only 0.5 eV in the LDA+U calculation. Therefore it is difficult to use that peak to extract the parameter $t_{\pi\pi}$ from the experimental spectra as it was done in Ref. 10. Furthermore, one should distinguish between different oxygen hopping matrix elements (t_{pp}, $t_{p\pi}$ and $t_{\pi\pi}$)[26] which was also not done there.[10]

B. Dispersion relations

The experimental spectra along both high symmetry directions show clear differences between both polarization directions (Figs. 7–10). The first electron removal peak along $\Gamma-(\pi,\pi)$ has minimal binding energy at $(\pi/2,\pi/2)$ and occurs exclusively with vertical polarization (Fig. 7). That is in
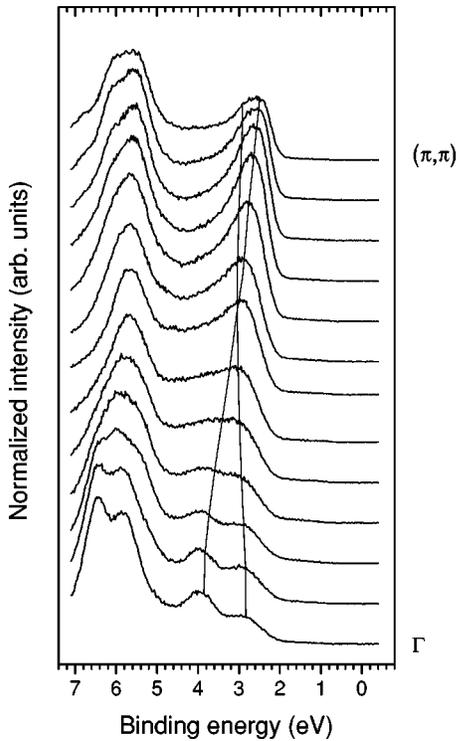
FIG. 8. Angle resolved photoemission curves along $\Gamma - (\pi, \pi)$ for horizontal polarization together with the calculated oxygen out-of-plane TB bands and the in-plane bands having even symmetry (calculated bands are shown as solid lines).
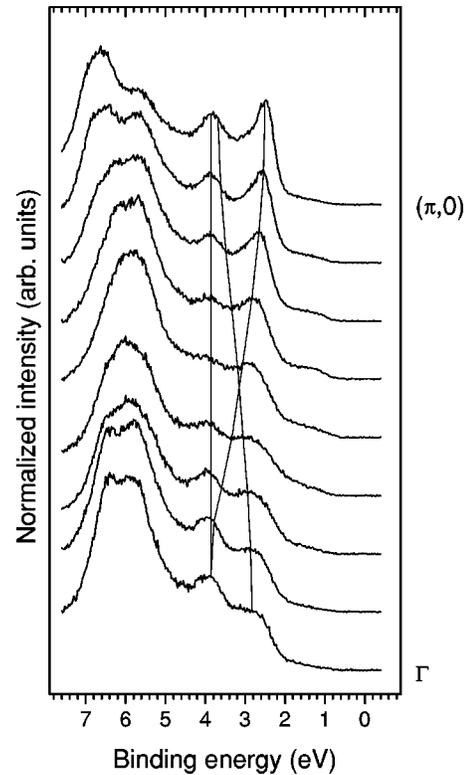
FIG. 10. Angle resolved photoemission curves along $\Gamma - (\pi, 0)$ for horizontal polarization with the calculated oxygen out-of-plane TB bands and the in-plane bands having even symmetry (calculated bands are shown as solid lines).
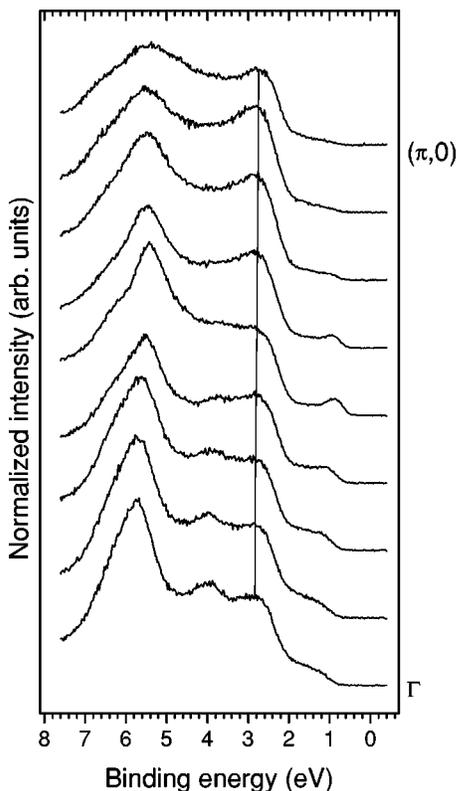
FIG. 9. Angle resolved photoemission curves along $\Gamma - (\pi, 0)$ for vertical polarization with the calculated antisymmetric oxygen TB band (shown as a solid line).

complete agreement with the usual interpretation of that peak as the Zhang-Rice singlet. In our mean-field treatment it is built up of the $d^{\downarrow}_{x^2-y^2}$ and p_{σ} orbitals having odd symmetry with respect to M_1. The dispersion is well described within the extended t-J model[9] and we have included the corresponding theoretical curve in Fig. 7 for completeness. Along $\Gamma - (\pi, 0)$ (Figs. 9 and 10) the Zhang-Rice singlet feature is less pronounced and according to our symmetry analysis based on a simple mean-field treatment we would expect it only with horizontal polarization. However, it is more clearly seen in Fig. 9 (vertical polarization) than in Fig. 10 (horizontal polarization). The explanation of that effect deserves obviously a more refined treatment and will be studied both theoretically and experimentally in the future.

The peak next in binding energy in Fig. 7 was already analyzed as the p_{π} orbital and it has a clear dispersion going from Γ to (π, π). The valence band edge at around 2.5 eV binding energy is different for both polarizations along $\Gamma - (\pi, 0)$ as well: it has no dispersion for vertical polarization (Fig. 9) and is built up of only one $(\widetilde{p}_{\pi})$ orbital. In contrast to that, we see for horizontal polarization (Fig. 10) one dispersionless out-of-plane band at 3.9 eV and two crossing bands from the out-of-plane orbitals and the in-plane p_{π} band.

To analyze this dispersion quantitatively it is more convenient to use the TB model than the LDA+U calculation due to the restricted number of bands in the former. The parameters of the TB model were found as follows. The LDA+U results at high symmetry points (Table III) were used to obtain a first parameter set. For the fit we have only chosen such energy levels which have no or very small con-

TABLE V. TB parameters (in eV) obtained by fitting the LDA+U band structure and the VB photoemission spectra. The off-site energies in parentheses are the values from a fit only to the theoretical band structure in the cases where experimental corrections were appropriate.

$\bar{\varepsilon}_d^{\uparrow}$	$\bar{\varepsilon}_d^{\downarrow}$	$\bar{\varepsilon}_{\bar{d}}$	$\bar{\varepsilon}_D$	$\bar{\varepsilon}_{d_z}$	$\bar{\varepsilon}_\pi$	$\bar{\varepsilon}_{p_z}$	$\bar{\varepsilon}_p$
2.00	-4.90	-4.78	-5.22	-6.40	-3.88	-3.86	-4.59

t_{pd}	$t_{p\bar{d}}$	t_{pp}	$t_{p\pi}$	$t_{\pi\pi}$	$t_{\pi D}$	t_{pdz}	
1.33	0.77	0.71	0.34	0.37	0.84	1.15	
				(0.32)	(0.77)	(0.77)	

tribution from other orbitals (Cu $4s$, O $3s$, Cl). In such a way our effective TB parameters also contain the influence of hybridization to Cl or s orbitals. Fitting to the pure LDA results (Table I) gave nearly the same hopping integrals but different on-site energies. The parameters are very similar to those known for La$_2$CuO$_4$.[34] After fitting to the LDA+U results there remained small differences to the experimental dispersions even for the peaks with lowest binding energy. These small discrepancies to the experimental peak positions were corrected by small changes of the on-site and off-site

FIG. 11. Position of the main experimental peaks together with the TB bands of the corresponding symmetry along $(\pi,0)-(0,0)-(\pi,\pi)$: (a) antisymmetric bands and experimental data for vertical polarization; (b) out-of-plane and symmetric bands together with experimental data for horizontal polarization. Full lines denote the TB bands with dominantly oxygen character, whereas the dashed lines correspond to bands with a considerable mixing to the copper system.

energies (here, especially t_{pdz} was increased). The resulting parameter set is shown in Table V.

In Fig. 11 we have collected all the peak positions from Figs. 7–10 together with the dispersion of the TB bands. We have distinguished between the results for vertical polarization [Fig. 11(a)] and horizontal polarization [Fig. 11(b)]. According to our previous analysis, the peaks in Fig. 11(a) between $(\pi,0)$ and Γ should only be compared with the 3 TB bands stemming from the $\tilde{p}_\sigma$, $\tilde{p}_\pi$, and d_{xy} orbitals. Analogously, between Γ and (π,π) [Fig. 11(a)] we present only the antisymmetric bands from the p_σ, p_π, $d_{x^2-y^2}^{\downarrow}$ and $d_{x^2-y^2}^{\uparrow}$ orbitals. In Fig. 11, we have collected the bands arising from both the $d_{x^2-y^2}^{\downarrow}$ or $d_{x^2-y^2}^{\uparrow}$ orbitals, and have neglected the band corresponding to the Zhang-Rice singlet since we cannot expect to obtain its correct dispersion in our simple mean-field treatment. The number of bands which contribute to the spectra for horizontal polarization [Fig. 11(b)] is considerably larger: these include all of the out-of-plane orbitals and additionally the corresponding symmetric bands (representation A_1 of C_{2v}) of the in-plane orbitals.

In Fig. 11 we have distinguished between bands with dominant oxygen character for all k values (solid lines) and those bands which have a considerable coupling to the copper spins (dashed lines). As one may note, there is a considerable agreement between experimental and theoretical dispersions for the oxygen bands with small binding energy. Furthermore, there is some similarity at the Γ point besides the peak with vertical polarization at 3.9 eV binding energy for which we have no explanation. But the copper bands at around 6 eV disperse strongly in the TB calculation whereas they are nearly dispersionless in the experiment. We think that this failure of the theoretical description arises due to the neglect of antiferromagnetic correlations. To avoid misunderstanding we should stress that also the oxygen bands of our mean-field calculation have a copper contribution (except some cases at the high-symmetry points), but that the copper contribution is not dominant. We have also shown the calculated dispersion relations of the oxygen bands in Figs. 7–10 as solid lines in order to guide the eye.

VII. CONCLUSIONS

It can be summarized that polarization dependent ARPES at Γ, (π,π) and $(\pi,0)$ and along the two high-symmetry directions gives detailed information about the bands with different parity with respect to reflections at the mirror planes M_1 and M_2. The assignment of the peaks can be performed by means of a symmetry analysis of band structure results. Here we pick out the three major results.

Rearrangement of energy levels. Comparing LDA with LDA+U results at high-symmetry points we found that the strong electron correlation leads to a changed order of energy levels, whereby the experimental peak positions could be more accurately assigned with the help of the LDA+U calculation. In comparison with an LDA calculation we found the copper bands shifted to higher binding energy. So, we conclude that the correlation influences not only the band near the Fermi level but leads to a rearrangement of energy levels throughout the whole VB.

Check of the nonbonding p_π band. Polarization dependent

ARPES measurements provide a sensitive test of the symmetries of the excitations with low binding energy which were already analyzed before. The p_π orbital is seen at (π,π) with vertical polarization as a single peak. At $(\pi,0)$ it is visible with horizontal polarization but overlaps with out-of-plane orbitals which makes a parameter assignment difficult. This means that in polarization independent measurement, such as those in Ref. 10, the spectral weight assigned to the p_π peak at (π,π) will have additional contributions besides the pure p_π orbital [of roughly one third of the total intensity as seen in Fig. 6(c)]. As a consequence, the experimental estimate of the spectral weight of the Zhang-Rice singlet part, which was performed there using the intensity of the p_π feature as a calibration, should be increased by 50%.

Dispersion relations. Analyzing the dispersion relations we observe a difference beween the copper bands which couple strongly to the antiferromagnetic spin structure and thus feel the antiferromagnetic BZ and the nonbonding oxygen bands which are decoupled from the spin system and follow the paramagnetic (or ferromagnetic) BZ. To take that effect into account for $Sr_2CuO_2Cl_2$ we should extend our theory twice. First we should incorporate the antiferromagnetic order. Then all the bands are defined within the AFM BZ. To obtain in such a scheme the observed difference between Γ and (π,π) deserves the calculation of matrix elements.

Despite the fact that the experimental order of energy levels can be explained by an LDA+U calculation one should be aware that the agreement between photoemission and LDA+U cannot be perfect. First of all, the LDA+U calculation cannot reproduce the satellite structure present in the spectra at about 14 eV binding energy. And second, the LDA+U has the tendency to push the copper levels to too large binding energy. That was visible in our analysis espe-cially at (π,π). The k-integrated copper density of states can also be measured by x-ray photoemission with large photon energy such that the copper cross section dominates that of oxygen.[35] It was found that the x-ray photoemission spectrum of the valence band of $Sr_2CuO_2Cl_2$ showed the existence of Cu $3d$ electron removal states over an energy range of some 5–6 eV. To compare our LDA+U calculation with earlier ones for La_2CuO_4,[17] one should also keep in mind that we had to choose a rather small shift of the copper levels to find agreement with the experimental situation, and we did not choose correlation parameters from a constrained density functional calculation as in Ref. 17. It can be expected that the consideration of self-energy corrections as was done recently by calculating the three-body scattering contributions[36,37] improves the situation and allows one to work with real correlation parameters instead of fitted ones. Our main goal here was the assignment of peaks and not the determination of parameters. To extract parameters from polarization dependent ARPES measurements there are several improvements necessary both from the experimental and the theoretical side of view.

APPENDIX

The TB matrix for the in-plane orbitals can be found in the form

	$d_{x^2-y^2}$	$d_{3z^2-r^2}$	d_{xy}	p_σ	p_π	$\tilde{p}_\sigma$	$\tilde{p}_\pi$
$d_{x^2-y^2}$	ε_d	0	0	$-2t_{pd}\lambda_q$	0	0	0
$d_{3z^2-r^2}$	0	$\varepsilon_{\tilde{d}}$	0	$t_{p\tilde{d}}\eta_q$	0	$t_{p\tilde{d}}\beta_q$	0
d_{xy}	0	0	ε_D	0	0	0	$t_{\pi D}\lambda_q$
p_σ	$-2t_{pd}\lambda_q$	$t_{p\tilde{d}}\eta_q$	0	$\varepsilon_p - t_{pp}\mu_q$	$t_{p\pi}\alpha_q$	$t_{pp}\nu_q$	0
p_π	0	0	0	$t_{p\pi}\alpha_q$	$\varepsilon_\pi - t_{\pi\pi}\mu_q$	0	$-t_{\pi\pi}\nu_q$
$\tilde{p}_\sigma$	0	$t_{p\tilde{d}}\beta_q$	0	$t_{pp}\nu_q$	0	$\varepsilon_p + t_{pp}\mu_q$	$-t_{p\pi}\alpha_q$
$\tilde{p}_\pi$	0	0	$t_{\pi D}\lambda_q$	0	$-t_{\pi\pi}\nu_q$	$-t_{p\pi}\alpha_q$	$\varepsilon_\pi + t_{\pi\pi}\mu_q$

where $s_{q,x}$, $s_{q,y}$, and λ_q are defined in the main text and the other expressions are given by

$$\mu_q = \frac{8s_{q,x}^2 s_{q,y}^2}{\lambda_q^2}, \qquad \nu_q = \frac{4s_{q,x}s_{q,y}(s_{q,x}^2 - s_{q,y}^2)}{\lambda_q^2},$$

$$\eta_q = \frac{s_{q,x}^2 - s_{q,y}^2}{\lambda_q}, \qquad \beta_q = \frac{2s_{q,x}s_{q,y}}{\lambda_q},$$

$$\alpha_q = 4\cos\left(\frac{q_x}{2}\right)\cos\left(\frac{q_y}{2}\right).$$

[1] M. Greven, R. J. Birgeneau, Y. Endoh, M. A. Kastner, B. Keimer, M. Matsuda, G. Shirane, and T. R. Thurston, Phys. Rev. Lett. **72**, 1096 (1994).

[2] B. O. Wells, Z.-X. Shen, A. Matsuura, D. M. King, M. A. Kastner, M. Greven, and R. J. Birgeneau, Phys. Rev. Lett. **74**, 964 (1995).

[3] S. La Rosa, I. Vobornik, F. Zwick, H. Berger, M. Grioni, G. Margaritondo, R. S. Keley, M. Onellion, and A. Chubukov, Phys. Rev. B **56**, 525 (1997).

[4] C. Kim, P. J. White, Z.-X. Shen, T. Tohyama, Y. Shibata, S. Maekawa, B. O. Wells, Y. J. Kim, R. S. Birgeneau, and M. A. Kastner, Phys. Rev. Lett. **80**, 4245 (1998).

[5] K. J. von Szczepanski, P. Horsch, W. Stephan, and M. Ziegler, Phys. Rev. B **41**, 2017 (1990).

[6] E. Dagotto, R. Joynt, A. Moreo, S. Bacci, and E. Gagliano, Phys. Rev. B **41**, 9049 (1990).

[7] R. Eder and K. Becker, Z. Phys. B **78**, 219 (1990).

[8] A. Nazarenko, K. J. E. Vos, S. Haas, E. Dagotto, and R. J. Gooding, Phys. Rev. B **51**, 8676 (1995).

[9] V. Yu. Yushankhai, V. S. Oudovenko, and R. Hayn, Phys. Rev. B **55**, 15 562 (1997).

[10] J. J. M. Pothuizen, R. Eder, N. T. Hien, M. Matoba, A. A. Menovsky, and G. A. Sawatzky, Phys. Rev. Lett. **78**, 717 (1997).

[11] J. G. Tobin, C. G. Olson, C. Gu, J. Z. Liu, F. R. Solal, M. J. Fluss, R. H. Howell, J. C. O' Brien, H. B. Radousky, and P. A. Sterne, Phys. Rev. B **45**, 5563 (1992).

[12] L. L. Miller, X. L. Wang, S. X. Wang, C. Stassis, D. C. Johnston, J. Faber, Jr., and C.-K. Loong, Phys. Rev. B **41**, 1921 (1990).

[13] H. C. Schmelz, M. S. Golden, S. Haffner, M. Knupfer, G. Krabbes, J. Fink, H. Rosner, R. Hayn, H. Eschrig, A. Müller, Ch. Jung, and G. Reichardt, Phys. Rev. B **57**, 10 936 (1998).

[14] W. E. Pickett, Rev. Mod. Phys. **61**, 433 (1989).

[15] J. P. Perdew and A. Zunger, Phys. Rev. B **23**, 5048 (1981).

[16] V. I. Anisimov, J. Zaanen, and O. K. Andersen, Phys. Rev. B **44**, 943 (1991).

[17] M. T. Czyzyk and G. A. Sawatzky, Phys. Rev. B **49**, 14 211 (1994).

[18] W. B. Peatman, J. Bahrdt, F. Eggenstein, G. Reichardt, and F. Senf, Rev. Sci. Instrum. **66**, 2801 (1995).

[19] J. J. Yeh and I. Lindau, At. Data Nucl. Data Tables **32**, 1 (1985). For 35 eV photons the corresponding cross sections are 9.4 Mb for Cu $3d$, 8.0 Mb for O $2p$, and 0.69 Mb for Cl $3p$.

[20] In fact there is a second mirror plane parallel to M_2 but going only through oxygen position. From the point of view of group theory it is identical to M_2 in the paramagnetic case.

[21] E.g., A. Zangwill, *Physics at Surfaces* (Cambridge University Press, Cambridge, England, 1988).

[22] H. Eschrig, *Optimized LCAO Method*, 1st ed. (Springer-Verlag, Berlin 1989).

[23] D. L. Novikov, A. J. Freeman, and J. D. Jorgensen, Phys. Rev. B **51**, 6675 (1995).

[24] D. J. Singh, *Planewaves, Pseudopotentials and the LAPW Method* Kluwer, Boston, 1994).

[25] H. Rosner, R. Hayn, and J. Schulenburg, Phys. Rev. B **57**, 13 660 (1998).

[26] L. F. Mattheiss and D. R. Hamann, Phys. Rev. B **40**, 2217 (1989).

[27] L. P. Bouckaert, R. Smoluchowski, and E. P. Wigner, Phys. Rev. **50**, 58 (1936).

[28] A. W. Luehrmann, Adv. Phys. **17**, 1 (1968).

[29] S. F. A. Kettle, *Symmetry and Structure* (Wiley, New York, 1995).

[30] M. S. Hybertsen, M. Schlüter, and N. E. Christensen, Phys. Rev. B **39**, 9028 (1989).

[31] The energy position and dispersion of the Zhang-Rice singlet are very sensitive to local AFM correlations which are well pronounced in the sample measured. To provide a correct description of the Zhang-Rice singlet (and its triplet partner) one has to subtract two orbitals, p_σ and $d_{x^2-y^2}$, from the 11-band manifold. Supplementary calculations for this two-band Hubbard model, done within the cell-perturbation method, led to a good account of the Zhang-Rice singlet dispersion measured (Ref. 9).

[32] It should be noted that even the pure oxygen bands have a small energy difference of 0.17 eV between both spin directions which is the same for all bands. The reason for that difference is the overlap between spin up and spin down at the Fermi energy. The position of spin down bands in Table III is corrected by this 0.17 eV.

[33] In fact, the oxygen in-plane wave functions have to be defined by the limit $k_x=k_y=k\rightarrow 0$ to have a defined parity with respect to M_1. In the limit $k_x=k\rightarrow 0$, $k_y=0$ they have a defined parity with respect to M_2. That arbitrariness can be explained since they build the two-dimensional representation E_u at the Γ point.

[34] M. S. Hybertsen, E. B. Stechel, M. Schluter, and D. R. Jennison, Phys. Rev. B **41**, 11 068 (1990).

[35] T. Boske, O. Knauff, R. Neudert, M. Kielwein, M. Knupfer, M. S. Golden, J. Fink, H. Eisaki, S. Uchida, K. Okada, and A. Kotani, Phys. Rev. B **56**, 3438 (1997).

[36] J. I. Igarashi, P. Unger, K. Hirai, and P. Fulde, Phys. Rev. B **49**, 16 181 (1994).

[37] M. Takahashi and J. Igarashi (unpublished).